Co-published by
Institute of Fluid-Flow Machinery
Polish Academy of Sciences
Committee on Thermodynamics and Combustion
Polish Academy of Sciences

Copyright©2026 by the Authors under licence CC BY-NC-ND 4.0

http://www.imp.gda.pl/archives-of-thermodynamics/

Analysis of oscillatory flow and heat transfer of Maxwell fluid through a porous circular microchannel with Hall effects

Muhammad Yousuf Rafiq, Zaheer Abbas, Ayesha Naeem*

The Islamia University of Bahawalpur, Baghdad-ul-Jadeed Campus, Hasilpur Road, Bahawalpur 63100, Pakistan
*Corresponding author email: ayeshanaeem432@gmail.com

Received: 30.07.2025; revised: 13.03.2026; accepted: 30.03.2026

Abstract

The oscillatory flow and heat transfer of a viscoelastic Maxwell fluid through a porous, rough circular microchannel are investigated in the presence of magnetohydrodynamic and Hall effects, velocity slip, and internal heat generation or absorption. The governing continuity, momentum and energy equations, coupled with the Maxwell constitutive relation, are formulated in cylindrical coordinates and non-dimensionalised. An analytical solution is obtained using the regular perturbation technique by treating wall roughness as a small parameter. Closed-form expressions for velocity and temperature are derived in terms of modified Bessel functions, and the shear stress and Nusselt number are evaluated. The results show that the magnetic parameter suppresses the axial velocity due to the Lorentz force, whereas the Hall parameter and Darcy number enhance the flow by alleviating electromagnetic and porous resistance. Velocity slip increases the near-wall velocity, while wall roughness reduces the overall flow intensity. Thermal analysis indicates that the temperature and Nusselt number increase with the heat source parameter and the Peclet number.

Keywords: Oscillatory flow; Maxwell fluid; Porous microchannel; Hall effect; Heat sink/source

Vol. 47(2026), No. 3, 125–137; doi: 10.24425/ather.2026.7509

Cite this manuscript as: Rafiq, M.Y., Abbas, Z., & Naeem, A. (2026). Analysis of oscillatory flow and heat transfer of Maxwell fluid through a porous circular microchannel with Hall effects. *Archives of Thermodynamics*, 47(3), 125–137.

1. Introduction

Oscillatory flow refers to the back-and-forth motion of fluid particles under the influence of periodic driving forces, commonly encountered in microfluidic and biological systems. This flow behaviour becomes particularly significant in confined geometries like microchannels, where inertial and elastic effects interact. The study of oscillatory flow helps understand complex transport phenomena in non-Newtonian fluids. It is widely applied in lab-on-chip devices, biomedical diagnostics, oil recovery, drug delivery systems, inkjet printing, chemical mixing processes, energy harvesting devices and thermal control systems. Ray et al. [1] conducted both analytical and numerical investigations to determine the development length of sinusoidally oscillating laminar pipe flows in moderate to high Reynolds number regimes. Astakhov et al. [2] investigated the phase reduction of a pair of coupled van der Pol oscillators subjected to an external harmonic force, incorporating asymmetric repulsive coupling between them. Aygun and Aydin [3,4] examined the hydrodynamics of piston-driven laminar pulsating flow for five dissimilar values of frequencies and compared the numerical and analytical solutions. Sato et al. [5] experimentally investigated the forced synchronisation of both the quasiperiodic state and the internally locked state in a thermoacoustic oscillator system. Aslan et al. [6] demonstrated the oscillatory flow and thermal features under the steady-state condition within a corrugated wavy channel. Additionally, three turbulence models were employed to examine the flow behaviour. Wang et al. [7] explored

Nomenclature

b – slip parameter
$\boldsymbol{B}$ – magnetic flux density vector, T
B_0 – magnitude of the applied uniform magnetic flux density, T
C_p – specific heat, J/(kg K)
Da – Darcy number
I_0, K_0 – zero-order modified Bessel functions of the first and second kind, respectively
$\boldsymbol{J}$ – current density, A/m^2
k – corrugation's wave number
k_p – permeability of porous medium, m^2
K – thermal conductivity, W/(m K)
m – Hall parameter
M – magnetic parameter
p – pressure, Pa
$P(t)$ – time-dependent oscillatory pressure gradient, Pa/m
Pe – Peclet number
Pr – Prandtl number
Q_0 – heat generation, W/m^3
r, θ, x – cylindrical coordinates (radial distance, angular coordinate, height)
R – mean radius, m
Re – Reynolds number
S – source/sink parameter
t – time, s
T – temperature, K
u_x – velocity component in x-direction, m/s
U – velocity, m/s
U_0 – characteristic velocity scale, m/s
$\boldsymbol{V}$ – velocity vector, m/s
$\widetilde{(\cdot)}$ – complex amplitude of the harmonically oscillating variable

Greek symbols

α – complex radial parameter
λ – relaxation time (Maxwell fluid parameter)
μ – dynamic viscosity, Pa·s
ν – kinematic viscosity, m^2/s
ξ – perturbation parameter (ratio of the wall-corrugation amplitude to the mean radius of the microchannel)
ρ – density, kg/m^3
σ – electrical conductivity, S/m
$\boldsymbol{\tau}$ – stress tensor, Pa
φ – amplitude of the pressure gradient
χ – generic dependent variable in the perturbation expansion
ω – oscillation frequency, rad/s

Abbreviations and Acronyms

MHD– magnetohydrodynamics
EOF – electroosmotic

the impact of rib shapes on oscillating flow and heat transfer in heat exchangers by deriving the solution numerically. Then, Li et al. [8] employed the perturbation technique to obtain the closed-form solution for the oscillating flow of Jeffrey fluid in a rough circular microchannel under the slip condition. Huang et al. [9] scrutinised the axial change of flow behaviour in the 3D rectangular channel with a deformable upper wall and compared the results with the experimental outcomes. The comparative examination of two-phase oscillatory flow with the experimental results was analysed by Duraziński et al. [10]. Yu et al. [11] discussed the impact of varying injecting angles on the flow behaviour and thermal features of liquid flow in the piston's galleries. Manthani et al. [12] examined the flow characteristics of a water-vinyl acetate system in the millichannel and computed the results numerically.

The flow of non-Newtonian fluids induced by surface motion plays a crucial role in various industrial and manufacturing processes due to their broad range of applications. Examples include optical fibre production, polymer processing, cooling of metallic surfaces and drilling operations. Since no single model can capture all the complex behaviours of non-Newtonian fluids, researchers have developed various models to better understand their rheological characteristics. Non-Newtonian fluids are generally classified into differential, rate-type and integral-type models. One of the significant non-Newtonian fluids is the Maxwell fluid. The Maxwell fluid is a fundamental viscoelastic non-Newtonian model that describes materials exhibiting both fluid-like and solid-like behaviour. It combines the effects of viscosity and elasticity through a linear relationship between stress and strain rate with a characteristic relaxation time. The Maxwell model is particularly useful for simulating fluids that undergo stress relaxation over time, such as polymer melts and biological fluids. Its ability to capture memory effects makes it ideal for studying unsteady and oscillatory flows in microfluidic and electrokinetic systems. Jian et al. [13,14] extended the study of Maxwell fluid in microchannels featuring different shapes under various circumstances. Li et al. [15] obtained an analytical solution for the transient electroosmotic velocity of generalised Maxwell fluids in a microchannel and a microtube, employing the Laplace technique. The outcomes were obtained by the linearised Poisson-Boltzmann equation along with the Cauchy momentum equation and the generalised Maxwell constitutive relation. Escandon et al. [16,17] demonstrated the transient EOFs (electroosmotic flows) of viscoelastic Maxwell fluids in microchannels with complex geometries, both annular and slit types, considering multilayer configurations and asymmetric zeta potentials. By employing analytical and partial-analytical techniques, they highlighted how elastic properties, electrokinetic effects and boundary asymmetries influence the oscillatory behaviour, symmetry and time evolution of velocity profiles in microfluidic systems. The unsteady magnetised flow of Maxwell fluids in a circular microchannel was analysed by Shah et al. [18] under an electric field depending on temperature, using the Debye-Hückel estimation. They derived the solution analytically and expressed the outcomes graphically. Yang et al. [19] investigated the unsteady oscillatory EOF flow of Maxwell fluid within a microchannel featuring an isosceles right triangular cross section. Due to the complexity of the problem, a numerical solution was derived. Feng et al. [20] introduced a fractional continuity model to scrutinise the gyrating EOF slip flow of generalised Maxwell fluids under an alternating electric field. The model captures the extended memory effects of viscoelastic fluids and provides insight into flow behaviour influenced by fractional dynamics and electrokinetic parameters.

Chang et al. [21] explored the electroosmotic flow (EOF) of a viscoelastic Maxwell fluid in a microchannel with sinusoidal wall unevenness, driven by an alternating pressure gradient and electric field. The effects of fluid elasticity, wall geometry, and external forcing on velocity distribution and mean flow behaviour were analytically investigated by using the Debye-Hückel approximation and boundary perturbation method.

Magnetohydrodynamics (MHD) examines the behaviour of electrically conducting fluids in the manifestation of a magnetic field, playing a vibrant role in numerous engineering and geophysical applications. The inclusion of the Hall effect is significant when the magnetic field is strong or the density of the fluid is low, causing a decoupling of electron and ion motion. This generates a secondary electric field perpendicular to both the magnetic and electric fields, which alters the current distribution and flow behaviour. Incorporating Hall currents in MHD analysis enhances the accuracy of modelling plasma flows, semiconductor processing and astrophysical phenomena. Jha et al. [22−25] investigated an MHD natural convection flow in vertical microchannels, highlighting the influence of Hall effects and induced magnetic fields. Their studies provide valuable insight into electromagnetic effects on microchannel heat and fluid transport under various magnetic field configurations. Roja and Gireesha [26] numerically investigated the MHD flow of a couple-stress fluid through a vertical microchannel, incorporating Hall effects and internal heat generation. Their study highlighted the impact of electromagnetic and thermal forces on non-Newtonian fluid behaviour in microchannel environments. Sadiq Basha et al. [27] analysed the steady MHD free convective flow in a vertical microchannel filled with a porous medium, considering Hall and ion-slip effects. Their study emphasised the impact of electromagnetic parameters on velocity and temperature profiles in microscale transport systems. Kundu and Saha [28] provided a comprehensive review of electromagnetohydrodynamic flow and heat transfer in microchannels, highlighting the interplay of electric and magnetic fields on fluid behaviour. Their analysis offers valuable insights into optimising thermal and flow performance in microscale systems. Bilal et al. [29] explored the unsteady flow of a hybrid nanofluid driven by peristaltic pumping in a wavy microchannel, incorporating the effects of electric and magnetic fields. Their study emphasised the role of Hall currents and slip boundary conditions, offering insights relevant to microfluidic and biomedical applications. Goyal and Srinivas [30] analysed the magnetic effect and entropy generation for the pulsating flow of two immiscible fluids, taking into consideration Joule heating and a first-order chemical reaction. They adopted the 4th-order Runge-Kutta numerical technique to evaluate the solution. Roja et al. [31] explored the influence of Hall effects on non-Newtonian fluid flow past an inclined microchannel under slip and convective boundary conditions. Their study provides valuable insights into electromagnetic and boundary interactions in complex fluid systems. Padma et al. [32] explored the magnetised flow of pulsating Casson fluid by considering the vertical porous medium along with slip conditions. They also discussed thermal features, including the entropy generation for the considered problem. Bala and Srinivas [33] scrutinised the magnetised flow of two incompressible Newtonian fluids over an inclined channel with the permeable medium and examined the thermal features incorporating the effect of heat flux, Joule heating and entropy generation. Srinivas et al. [34] examined the periodic pressure gradient and thermal features of the pulsatile and peristaltic flow of a particle fluid. They observed that the variations in pressure enhanced the fluid mixing, improving the thermal characteristics within the medium.

The literature review reveals a lack of studies on Maxwell fluid in a rough circular channel. Therefore, the main motivation behind this work is to analyse the magnetised flow of a Maxwell fluid under the influence of the Hall effect within a porous, rough circular microchannel. Additionally, the thermal characteristics of the fluid are also scrutinised in the presence of the heat sink/source parameter. The analytical solution for velocity and temperature is derived by the perturbation technique. The inspiration for the current study is the practical application of non-Newtonian fluid flow in rough circular microchannels, e.g. in biomedical devices, such as lab-on-a-chip systems and targeted drug delivery, microelectronics, oil and gas industries, and in chemical microreactors, etc. The impact of key parameters on the velocity and temperature is discussed graphically, while the effects on shear stress and Nusselt number are described in tabular form.

2. Problem formulations

The current work explores the oscillatory flow of a magnetised Maxwell fluid within a rough circular porous microchannel under the influence of the Hall effect and slip boundary conditions. The thermal characteristics of the fluid are also examined with the effect of thermal radiation and a heat sink/source. A cylindrical polar coordinate system (r, θ, x) is used to indicate the radial direction, azimuthal direction and central axis, respectively, as demonstrated in Fig. 1. The flow occurs due to an oscillatory pressure gradient with the uniform magnetic field acting perpendicular to the axial direction. A sinusoidal wave of slight amplitude is assumed to represent the corrugation of wall roughness and can be stated as

$$r = R + R\xi \sin(k\theta), \tag{1}$$

where R signifies the mean radius, k is the corrugation's wave number, and ξ ($\xi \ll 1$) is the perturbation parameter defined as the ratio of the amplitude of wall corrugations to the mean radius of the microchannel.

The flow governing equations are given by:

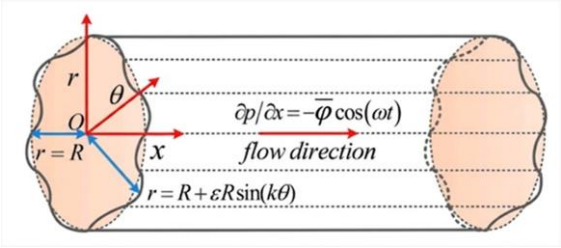


Fig. 1. Schematic diagram of the problem.

$$\nabla \cdot \boldsymbol{V} = 0, \tag{2}$$

$$\rho \frac{\partial \boldsymbol{V}}{\partial t} = -\nabla \cdot (p\mathbf{I} + \boldsymbol{\tau}) + \frac{\boldsymbol{J}\times\boldsymbol{B}}{1+m^2} + \frac{\mu}{k_p}, \tag{3}$$

$$\rho C_p \left(\frac{\partial T}{\partial t} + \boldsymbol{V} \cdot \nabla T\right) = K\nabla^2 T + Q_0, \tag{4}$$

where $\boldsymbol{V}$ is the velocity vector, $\boldsymbol{B}$ signifies magnetic field strength, $\boldsymbol{J}$ is the current density, $\mathbf{I}$ is the identity tensor, $\boldsymbol{\tau}$ is the stress tensor, m is the Hall parameter, ρ designates the density, K symbolises the thermal conductivity, C_p is the specific heat at constant pressure, T is the temperature, p indicates pressure, t is the time, Q_0 is the heat source/sink, and μ describes the dynamic viscosity. The stress tensor for an incompressible Maxwell fluid is given by

$$\boldsymbol{\tau} + \lambda \frac{D\boldsymbol{\tau}}{Dt} = 2\mu\mathbf{A}, \tag{5}$$

where λ is the relaxation time (a Maxwell fluid parameter), $\frac{D}{Dt}$ is the material derivative, and $\mathbf{A} = \frac{1}{2}(\nabla\boldsymbol{V} + \nabla\boldsymbol{V}^T)$ represents the rate-of-strain tensor. Under the assumed conditions, the stress tensor for the Maxwell fluid is simplified as

$$\left(1 + \lambda\frac{\partial}{\partial t}\right)\tau_{rx} = \mu\frac{\partial u_x}{\partial r}. \tag{6}$$

where τ_{rx} is the shear stress in the x-direction on a constant r-plane, and u_x denotes the velocity component in x-direction.

The time-dependent velocity field is taken as

$$\boldsymbol{V} = \big(0,0,u_x(r,\theta,t)\big). \tag{7}$$

The normal magnetic field is applied in the direction opposite to the direction of motion, which, according to Ohm's law, gives

$$\boldsymbol{J}\times\boldsymbol{B} = (0,0,-\sigma B_0^2 u_x), \tag{8}$$

where σ denotes electrical conductivity and B_0 is the magnitude of the applied magnetic flux density.

According to the above-mentioned assumptions, the governing equations are reduced to

$$\left(1 + \lambda\frac{\partial}{\partial t}\right)\left(\rho\frac{\partial u_x}{\partial t} + \frac{\partial p}{\partial x}\right) = \mu\left(\frac{\partial^2 u_x}{\partial r^2} + \frac{1}{r}\frac{\partial u_x}{\partial r} + \frac{1}{r^2}\frac{\partial^2 u_x}{\partial\theta^2}\right) + \\ -\frac{\mu}{k_p}u_x + \frac{-\sigma B_0^2 u_x}{1+m^2}, \tag{9}$$

$$\rho C_p\frac{\partial T}{\partial t} = K\left(\frac{\partial^2 T}{\partial r^2} + \frac{1}{r}\frac{\partial T}{\partial r} + \frac{1}{r^2}\frac{\partial^2 T}{\partial\theta^2}\right) + Q_0, \tag{10}$$

$$u_x|_{r=0} < \infty, \qquad T|_{r=0} < \infty,$$
$$\left(u_x + b\frac{\partial u_x}{\partial r}\right)\Big|_{r=R+\xi R\sin(k\theta)} = 0, \quad T|_{r=R+\xi R\sin(k\theta)} = 0, \tag{11}$$

where b is the slip parameter.

The expressions for pressure gradient, velocity and temperature in the x-direction for the oscillations in the form of a complex function are obtained as:

$$\frac{\partial p}{\partial x} = -P(t) = -\varphi\cos(\omega t) = -\varphi\Re\{e^{i\omega t}\}, \tag{12}$$

$$u_x(r,\theta,t) = \Re\{\tilde{u}(r,\theta)e^{i\omega t}\}, \tag{13}$$

$$T(r,\theta,t) = \Re\{\tilde{T}(r,\theta)e^{i\omega t}\}, \tag{14}$$

where $\Re\{\cdot\}$ shows the real part, ω is the angular frequency of oscillation, and φ represents the amplitude of a pressure gradient, $P(t)$ denotes the time-dependent oscillatory pressure gradient, and $\widetilde{(\cdot)}$ denotes the complex amplitude of the corresponding harmonically oscillating variable.

Inserting Eqs. (12)–(14) into Eqs. (9)–(11) yields:

$$i\omega\tilde{u}(r,\theta) = \left[\frac{\partial^2\tilde{u}(r,\theta)}{\partial r^2} + \frac{1}{r}\frac{\partial\tilde{u}(r,\theta)}{\partial r} + \frac{1}{r^2}\frac{\partial^2\tilde{u}(r,\theta)}{\partial\theta^2}\right]\left(\frac{\nu}{1+i\omega\boldsymbol{\lambda}}\right) + \\ + \frac{-\sigma B_0^2\tilde{u}}{1+m^2} - \frac{\mu}{k_p}\tilde{u} + \frac{\varphi}{\rho}, \tag{15}$$

$$\rho C_p i\omega\tilde{T}(r,\theta) = K\left[\frac{\partial^2\tilde{T}(r,\theta)}{\partial r^2} + \frac{1}{r}\frac{\partial\tilde{T}(r,\theta)}{\partial r} + \frac{1}{r^2}\frac{\partial^2\tilde{T}(r,\theta)}{\partial\theta^2}\right] + Q_0, \tag{16}$$

where $\nu = \mu/\rho$ is the kinematic viscosity.

The reduced boundary conditions are:

$$\tilde{u}|_{r=0} < \infty, \qquad \tilde{T}\big|_{r=0} < \infty,$$
$$\left(\tilde{u} + b\frac{\partial\tilde{u}}{\partial r}\right)\Big|_{r=R+\xi R\sin(k\theta)} = 0, \quad \tilde{T}\big|_{r=R+\xi R\sin(k\theta)} = 0. \tag{17}$$

The non-dimensional variables are defined as

$$r^* = \frac{r}{R}, \qquad t^* = \omega t, \qquad u^*(r^*,\theta) = \frac{\tilde{u}(r,\theta)}{U_0}, \\ b^* = \frac{b}{R}, \qquad \lambda^* = \omega\lambda, \qquad T^*(r^*,\theta) = \frac{\tilde{T}-T_0}{T_1-T_0}, \\ M = \sqrt{\frac{\sigma\omega}{\mu}}RB_0, \quad \mathrm{Da} = \frac{k_p}{r^2}, \qquad \mathrm{Re} = \frac{R^2\omega}{\nu}, \\ \mathrm{Pr} = \frac{C_p\mu}{K}, \qquad \mathrm{Pe} = \mathrm{Pr}R, \qquad S = \frac{R\omega Q_0}{T_1-T_0}, \tag{18}$$

where U_0 is the characteristic velocity scale, M is the magnetic parameter, Da denotes Darcy number, Pr – Prandtl number, Re – Reynolds number, Pe – Peclet number, S is the source parameter, T_0 and T_1 are the reference temperatures used for nondimensionalisation, and T_1–T_0 represents the characteristic temperature difference.

After removing the stearic signs for simplification, Eqs. (15) and (16) in non-dimensional form are reduced as

$$\frac{\partial^2 u}{\partial r^2} + \frac{1}{r}\frac{\partial u}{\partial r} + \frac{1}{r^2}\frac{\partial^2 u}{\partial\theta^2} - \left(i\mathrm{Re} + \frac{M^2}{1+m^2} + \frac{1}{\mathrm{Da}}\right)(1+i\lambda)u + \\ +(1+i\lambda)\varphi = 0, \tag{19}$$

$$\mathrm{Pe}\,T = \frac{\partial^2 T}{\partial r^2} + \frac{1}{r}\frac{\partial T}{\partial r} + \frac{1}{r^2}\frac{\partial^2 T}{\partial\theta^2} + S. \tag{20}$$

The dimensionless boundary conditions are defined as

$$u|_{r=0} < \infty, \qquad T|_{r=0} < \infty,$$
$$\left(u + b\frac{\partial u}{\partial r}\right)\Big|_{r=1+\xi\sin(k\theta)} = 0, \quad T|_{r=1+\xi\sin(k\theta)} = 0. \tag{21}$$

3. Analytic solution

As Eqs. (19) and (20) are the second-order partial differential equations (PDE's), the perturbation technique is employed to derive the solution by assuming the perturbation parameter $\xi \ll 1$

$$\chi(r,\theta) = \chi_0(r) + \xi\chi_1(r,\theta) + \xi^2\chi_2(r,\theta) + \cdots, \quad (22)$$

where the velocity and temperature are collectively represented by χ.

The zero, first, and second order equations in velocity and temperature are derived from Eqs. (19) and (20) as

$$\frac{d^2u_0}{dr^2} + \frac{1}{r}\frac{du_0}{dr} - \alpha^2 u_0 + \frac{1}{A}\alpha^2\chi = 0, \quad (23)$$

$$\mathrm{Pe}\, T_0 = \frac{d^2T_0}{dr^2} + \frac{1}{r}\frac{dT_0}{dr} + S, \quad (24)$$

$$\frac{\partial^2u_1}{\partial r^2} + \frac{1}{r}\frac{\partial u_1}{\partial r} + \frac{1}{r}\frac{\partial^2u_1}{\partial\theta^2} - \alpha^2 u_1 = 0, \quad (25)$$

$$\mathrm{Pe}\, T_1 = \frac{\partial^2T_1}{\partial r^2} + \frac{1}{r}\frac{\partial T_1}{\partial r} + \frac{1}{r}\frac{\partial^2T_1}{\partial\theta^2}, \quad (26)$$

$$\frac{\partial^2u_2}{\partial r^2} + \frac{1}{r}\frac{\partial u_2}{\partial r} + \frac{1}{r}\frac{\partial^2u_2}{\partial\theta^2} - \alpha^2 u_2 = 0, \quad (27)$$

$$\mathrm{Pe}\, T_2 = \frac{\partial^2T_2}{\partial r^2} + \frac{1}{r}\frac{\partial T_2}{\partial r} + \frac{1}{r}\frac{\partial^2T_2}{\partial\theta^2}, \quad (28)$$

where

$$\alpha^2 = (1+i\lambda)\left(i\mathrm{Re} + \frac{M^2}{1+m^2} + \frac{1}{\mathrm{Da}}\right)$$

and

$$A = i\mathrm{Re} + \frac{M^2}{1+m^2} + \frac{1}{\mathrm{Da}}.$$

By applying Taylor's series, the slip boundary condition along $r = 1$ is expanded as

$$0 = \left[u_0 + b\frac{du_0}{dr}\right]\Big|_{r=1} + \xi\left[u_1 + b\frac{\partial u_1}{\partial r} + \sin(k\theta)\left(\frac{du_0}{dr} + b\frac{d^2u_0}{dr^2}\right)\right]\Big|_{r=1} +$$

$$+\xi^2\left[u_2 + b\frac{\partial u_2}{\partial r} + \sin(k\theta)\left(\frac{\partial u_1}{\partial r} + b\frac{\partial^2u_2}{\partial r^2}\right) + \frac{\sin^2(k\theta)}{2}\left(\frac{d^2u_0}{dr^2} + b\frac{d^3u_0}{dr^3}\right)\right]\Big|_{r=1} + \mathrm{O}(\xi^3), \quad (29)$$

$$0 = T_0|_{r=1} + \xi\left[T_1 + \sin(k\theta)\frac{dT_0}{dr}\right]\Big|_{r=1} + \xi^2\left[T_2 + \sin(k\theta)\frac{\partial T_1}{\partial r} + \frac{\sin^2(k\theta)}{2}\frac{d^2T_0}{dr^2}\right]\Big|_{r=1} + \mathrm{O}(\xi^3). \quad (30)$$

The related boundary conditions are

$$\xi^0\begin{cases} u_0|_{r=1} = -b\frac{du_0}{dr}\Big|_{r=1}, & |u_0|_{r=0}| < \infty, \\ T_0|_{r=1} = 0, & |T_0|_{r=0}| < \infty, \end{cases} \quad (31)$$

$$\xi^1\begin{cases} u_1|_{r=1} = -\sin(k\theta)\left(\frac{du_0}{dr} + b\frac{d^2u_0}{dr^2}\right)\Big|_{r=1} - b\frac{\partial u_1}{\partial r}\Big|_{r=1}, & |u_1|_{r=0}| < \infty, \\ T_1|_{r=1} = -\sin(k\theta)\left(\frac{dT_0}{dr}\right)\Big|_{r=1}, & |T_1|_{r=0}| < \infty, \end{cases} \quad (32)$$

$$\xi^2\begin{cases} u_2|_{r=1} = -\sin(k\theta)\left(\frac{\partial u_1}{\partial r} + b\frac{\partial^2u_1}{\partial r^2}\right)\Big|_{r=1} - \frac{\sin^2(k\theta)}{2}\left(\frac{d^2u_0}{dr^2} + b\frac{d^3u_0}{dr^3}\right)\Big|_{r=1} - b\frac{\partial u_2}{\partial r}\Big|_{r=1}, & |u_2|_{r=0}| < \infty, \\ T_2|_{r=1} = -\sin(k\theta)\left(\frac{\partial T_1}{\partial r}\right)\Big|_{r=1} - \frac{\sin^2(k\theta)}{2}\left(\frac{d^2T_0}{dr^2}\right)\Big|_{r=1}, & |T_2|_{r=0}| < \infty. \end{cases} \quad (33)$$

3.1. Zero-order solution

The zero-order velocity and temperature equations, together with their corresponding boundary conditions, are obtained from Eqs. (23), (24) and (31) as follows

$$\begin{cases} \frac{d^2u_0}{dr^2} + \frac{1}{r}\frac{du_0}{dr} - \alpha^2 u_0 + \frac{1}{A}\alpha^2\chi = 0, \\ u_0|_{r=1} = -b\frac{du_0}{dr}\Big|_{r=1}, \quad |u_0|_{r=0}| < \infty, \end{cases} \quad (34)$$

$$\begin{cases} \mathrm{Pe}\, T_0 = \frac{d^2T_0}{dr^2} + \frac{1}{r}\frac{dT_0}{dr} + S, \\ T_0|_{r=1} = 0, \qquad |T_0|_{r=0}| < \infty. \end{cases} \quad (35)$$

The solution of Eqs. (34) and (35) is obtained in the form of a Bessel function with the imaginary argument as

$$u_0(r) = \frac{1}{A}\varphi + B_1 I_0(0, r\alpha) + B_2 K_0(0, r\alpha), \quad (36)$$

$$T_0(r) = \frac{S}{\mathrm{Pe}} + B_3 I_0\left(0, \sqrt{\mathrm{Pe}}\, r\right) + B_4 K_0\left(0, \sqrt{\mathrm{Pe}}\, r\right), \quad (37)$$

where I_0 and K_0 are the zero-order modified Bessel functions of the first and second kind, respectively.

Substituting the condition $|u_0|_{r=0}| < \infty$ and $|T_0|_{r=0}| < \infty$ in Eq. (36) and (37) gives $B_2 = 0$ and $B_4 = 0$. Further, applying the boundary conditions from Eqs. (34) and (35) gives

$$B_1 = -\frac{\varphi}{A[I_0(0,\alpha) + b\xi I_0[1,\alpha]]}, \quad (38)$$

$$B_3 = -\frac{S}{\mathrm{Pe}\, I_0\left(0, \sqrt{\mathrm{Pe}}\right)}. \quad (39)$$

and the zero-order velocity and temperature take the form:

$$u_0(r) = \frac{1}{A}\varphi + B_1 I_0(0, r\alpha) =$$

$$= \frac{1}{A}\varphi\left[1 - \frac{I_0(0,r\alpha)}{I_0(0,\alpha)+b\alpha I_0(1,\alpha)}\right], \quad (40)$$

$$T_0(r) = \frac{S}{\mathrm{Pe}}\left[1 - \frac{I_0[0,\sqrt{\mathrm{Pe}}\, r]}{I_0[0,\sqrt{\mathrm{Pe}}]}\right]. \quad (41)$$

3.2. First order solution

Similar to the zero-order formulation, the first-order velocity and temperature equations, along with boundary conditions, are:

$$\begin{cases} \frac{\partial^2 u_1}{\partial r^2} + \frac{1}{r}\frac{\partial u_1}{\partial r} + \frac{1}{r}\frac{\partial^2 u_1}{\partial \theta^2} - \alpha^2 u_1 = 0, \\ u_1|_{r=1} = \left[\sin(k\theta)\left(\frac{-du_0}{dr} - b\frac{d^2u_0}{dr^2}\right) - b\frac{\partial u_1}{\partial r}\right]\Big|_{r=1}, \\ |u_1|_{r=0}| < \infty, \end{cases} \quad (42)$$

$$\begin{cases} \mathrm{Pe}\, T_1 = \frac{\partial^2 T_1}{\partial r^2} + \frac{1}{r}\frac{\partial T_1}{\partial r} + \frac{1}{r}\frac{\partial^2 T_1}{\partial \theta^2}, \\ T_1|_{r=1} = -\sin(k\theta)\frac{dT_0}{dr}, \qquad |T_1|_{r=0}| < \infty. \end{cases} \quad (43)$$

The method of separation of variables derives the final expression for the first-order velocity and temperature as

$$u_1(r,\theta) = C_6 \sin(k\theta)\, I_0(k, r\alpha) =$$

$$-[b\alpha I_0(0,\alpha) - (-1+b)\, I_0(1,\alpha)] \times \frac{B_1\alpha \sin(k\theta) I_0(k,r\alpha)}{(1+kb)I_0(k,\alpha)+b\alpha I_0(k+1,\alpha)}, \quad (44)$$

$$T_1(r) = D_6 \sin(k\theta)\, I_0\left(k, \sqrt{\mathrm{Pe}}\, r\right) =$$

$$= -\frac{\sqrt{\mathrm{Pe}}\, I_0(1,\sqrt{\mathrm{Pe}}) B_3 \sin(k\theta) I_0(k,\sqrt{\mathrm{Pe}}\, r)}{I_0(k,\sqrt{\mathrm{Pe}})}, \quad (45)$$

where B_1 and B_3 are the zero-order integration constants defined in Eqs. (38) and (39), respectively, while C_6 and D_6 are the first-order constants determined by applying the boundary conditions in Eqs. (42) and (43).

3.3. Second order solution

The governing equations and boundary conditions for the second-order problem are:

$$\begin{cases} \frac{\partial^2 u_2}{\partial r^2} + \frac{1}{r}\frac{\partial u_2}{\partial r} + \frac{1}{r}\frac{\partial^2 u_2}{\partial \theta^2} - \alpha^2 u_2 = 0, \\ u_2|_{r=1} = -\sin(k\theta)\left(\frac{\partial u_1}{\partial r} + b\frac{\partial^2 u_1}{\partial r^2}\right)\Big|_{r=1} - \frac{\sin^2(k\theta)}{2}\left(\frac{d^2u_0}{dr^2} + b\frac{d^3u_0}{dr^3}\right)\Big|_{r=1} - b\frac{\partial u_2}{\partial r}\Big|_{r=1}, \qquad |u_2|_{r=0}| < \infty. \end{cases} \quad (46)$$

$$\begin{cases} \mathrm{Pe}\, T_2 = \frac{\partial^2 T_2}{\partial r^2} + \frac{1}{r}\frac{\partial T_2}{\partial r} + \frac{1}{r}\frac{\partial^2 T_2}{\partial \theta^2}, \\ T_2|_{r=1} = -\sin(k\theta)\left(\frac{\partial T_1}{\partial r}\right)\Big|_{r=1} - \frac{\sin^2(k\theta)}{2}\frac{d^2T_0}{dr^2}\Big|_{r=1}, \qquad |T_2|_{r=0}| < \infty. \end{cases} \quad (47)$$

Similarly to zero and first order solution, the second order solution is also finalised on the similar pattern as

$$u_2(r,\theta) = E_3 \cos(2k\theta)\, I_0(2k, r\alpha) + E_5 I_0(0, r\alpha) = \frac{2B_6D_1 + A_1D_2}{4}\left[\frac{I_0(2k,r\alpha)\cos(2k\theta)}{(1-2kb)I_0(2k,\alpha)+b\alpha I_0(1+2k,\alpha)} - \frac{I_0(0,r\alpha)}{I_0(0,\alpha)+b\alpha I_0(1,\alpha)}\right], \quad (48)$$

$$T_2(r,\theta) = F_3 \cos(2k\theta)\, I_0\left(2k, \sqrt{\mathrm{Pe}}\, r\right) + F_5 I_0\left(0, \sqrt{\mathrm{Pe}}\, r\right) = \frac{2C_6E_1 + A_3E_2}{4}\left[\frac{I_0\left(2k,\sqrt{\mathrm{Pe}}\, r\right)\cos(2k\theta)}{I_0\left(2k,\sqrt{\mathrm{Pe}}\right)} + \frac{I_0\left(0,\sqrt{\mathrm{Pe}}\, r\right)}{I_0\left(2k,\sqrt{\mathrm{Pe}}\right)+b\alpha I_0\left(0,\sqrt{\mathrm{Pe}}\right)}\right], \quad (49)$$

where A_1, A_3, B_6, C_6, D_1, D_2, E_1, E_2, E_3, E_5, F_3 and F_5 are auxiliary/integration constants arising from the perturbation solution and boundary condition algebra. C_6 is inherited from the first-order solution, while the remaining constants used at second order are fixed by the corresponding conditions in Eqs. (46) and (47).

3.4. Approximate analytical solution

The approximate analytic solution of velocity and temperature takes the form:

$$u(r,\theta) = A - \frac{AI_0(0,r\alpha)}{I_0(0,\alpha)+b\alpha I_0(1,\alpha)} - \xi I_0(k, r\alpha) B_1\alpha \sin(k\theta)\left[\frac{B_1\alpha \sin(k\theta) I_0(k,r\alpha)}{(1+kb)I_0(k,\alpha)+b\alpha I_0(k+1,\alpha)}\right] +$$

$$+ \frac{2B_6D_1 + A_1D_2}{4}\left[\frac{I_0(2k,r\alpha)\cos(2k\theta)}{(1-2kb)I_0(2k,\alpha)+b\alpha I_0(1+2k,\alpha)} - \frac{I_0(0,r\alpha)}{I_0(0,\alpha)+b\alpha I_0(1,\alpha)}\right], \quad (50)$$

$$T(r,\theta) = \frac{S}{\mathrm{Pe}} + \left[1 - \frac{I_0\left(0,\sqrt{\mathrm{Pe}}\, r\right)}{I_0\left(0,\sqrt{\mathrm{Pe}}\right)}\right] A_3 \sin(k\theta)\left[\frac{\xi I_0\left(1,\sqrt{\mathrm{Pe}}\right) I_0\left(k,\sqrt{\mathrm{Pe}}\, r\right)}{I_0\left(k,\sqrt{\mathrm{Pe}}\right)}\right] + \left(\frac{2D_6F_1 + B_3F_2}{4}\right)\xi^2\left[\frac{I_0\left(2k,\sqrt{\mathrm{Pe}}\, r\right)\cos(2k\theta)}{I_0\left(2k,\sqrt{\mathrm{Pe}}\, r\right)} + \frac{I_0\left(0,\sqrt{Pe}\, r\right)}{I_0\left(0,\sqrt{\mathrm{Pe}}\right)}\right]. \quad (51)$$

where ξ is the perturbation parameter representing the dimensionless wall roughness. It is substantial to mention that if the wall roughness is neglected, i.e. $\xi = 0$, then the problem is reduced from a rough circular channel to a smooth one.

4. Shear stress

The wall shear stress for unidirectional incompressible flow, where the tangential stress at the channel wall is proportional to

the radial gradient of the axial velocity, can be expressed mathematically as

$$\tau = \left.\frac{\partial u}{\partial r}\right|_{r=1}, \tag{52}$$

which can be obtained by differentiating the approximate velocity solution and evaluating it at $r = 1$.

5. Nusselt number

The dimensionless Nusselt number to determine the rate of heat transfer is obtained from the approximate temperature solution evaluated at the wall (Eq. (51)):

$$\mathrm{Nu}(r) = -\left.\frac{\partial T}{\partial r}\right|_{r=1}. \tag{53}$$

6. Observations and discussion

The current study presents the closed-form solution of magnetised flow of Maxwell fluid along with the Hall effect in a porous, rough circular microchannel with slip boundary conditions. The thermal characteristics of the flow in the presence of a heat source are analysed in detail. The perturbation technique is applied to derive the solution, which is found in the form of a Bessel function. The impact of controlling parameters on the fluid's velocity and temperature is given graphically. Additionally, the impact of the fluid parameter, Darcy number and Hall parameter, on shear stress and the influence of the source parameter and Peclet number on the Nusselt number are shown in tabular form. The characteristics of oscillatory flow are dominantly affected by the frequency parameter, which is represented by the angular Reynolds number. At low frequencies, the viscous forces are dominant, and the fluid is able to completely relax the oscillatory pressure gradient, resulting in a smooth velocity profile and an increased flow rate. However, at higher frequencies, the inertial forces become more pronounced, leading to a reduction in velocity magnitude due to the limited diffusion of momentum in the channel. Additionally, higher frequencies cause a phase lag between the velocity and the applied pressure gradient. In circular microchannels, this results in the development of annular velocity profiles and backflow regions. The slip at the wall becomes less effective with increasing frequency due to the dominance of oscillatory inertia. Wall roughness further disrupts the flow at higher frequencies, leading to an increase in near-wall fluctuations and a reduction in the overall transport. As a result, the flow rate decreases with increasing frequency.

The accuracy and reliability of the present work was validated through a comparison of the obtained velocity profiles with those of the previous study by Li et al. [8].

6.1. Velocity distribution

Figures 2–4 show the impact of different parameters on the velocity profile of a Maxwell fluid, while Figs. 5–7 depict the velocity contours for the variation of the relaxation time (λ), the Darcy number (Da) and the magnetic parameter (M), respectively. Figure 2a represents the effect of amplitude (φ) on velocity, showing that the velocity increases with increasing φ . This is because the oscillatory motion rises with the increment in amplitude, inducing an inclination in the fluid's motion. The influence of the slip parameter (b) on the velocity profile is portrayed in Fig. 2b. It is noted that velocity rises near the wall of the microchannel, and overall velocity also increases with increasing the slip parameter, as the upsurge in b induces a decline in the friction at the wall, causing an ease for the fluid flow due to the slip condition. Figure 3a explains the impact of the relaxation time (λ) on the velocity distribution. It is perceived that the velocity profile enhances significantly with the rise in λ. Physically, an increase in λ causes a strong elastic behaviour of the fluid and delayed relaxation, which aids the propagation of oscillatory flow, causing an increment in the liquid motion. As can be seen from Fig. 3b, as the perturbation parameter (ξ) increases, more energy is dissipated near the wall due to enhanced resistance or irregular surface interaction. This leads to increased friction and momentum loss in the fluid layers. As a consequence, the axial velocity decreases throughout the channel. Additionally, the disturbance disrupts the smooth flow pattern, further reducing the net flow efficiency. Therefore, a higher perturbation parameter suppresses velocity due to dominant damping and resistance effects.

Figure 4a illustrates the impact of magnetic parameter (M) on the fluid flow showing that velocity declines with an increase in the magnetic effect. It is because, this effect attributed towards Lorentz force acts as a resistive force to the flow, causing a dampness in the flow. Figure 4b implies that the velocity profile enhances with the rise in Hall effect. The increment in Hall

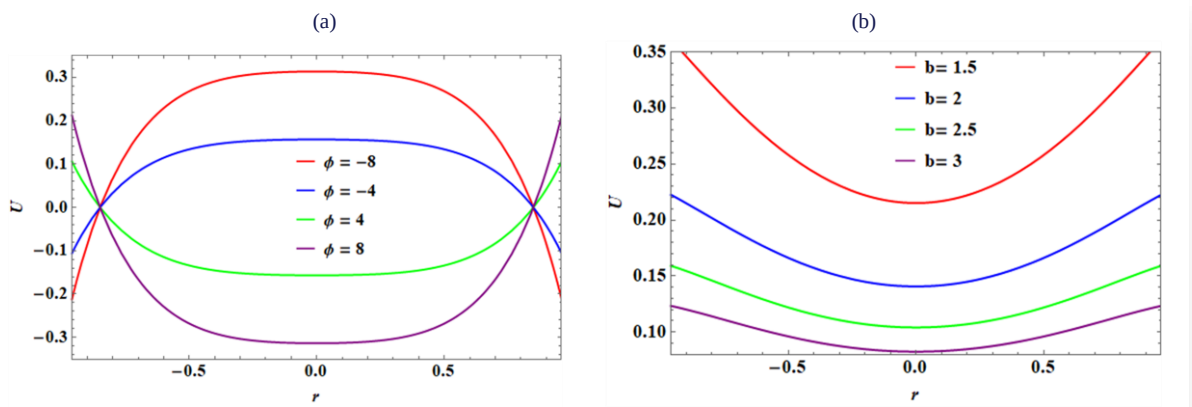


Fig. 2. Velocity profile change with amplitude (a) and slip parameter (b).

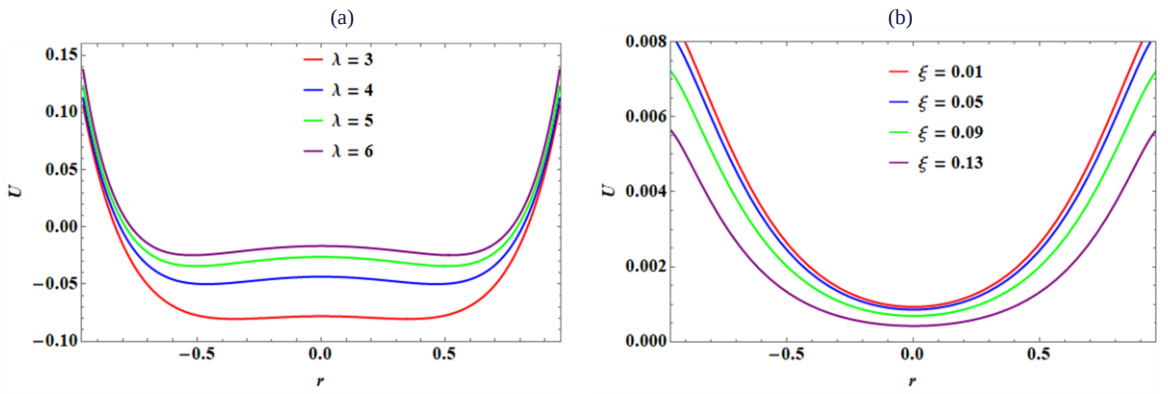


Fig. 3. Change of the velocity profile with the relaxation time (a) and perturbation parameter (b).

effect leads to the decline in electrical conductivity generation, which opposes the dampness caused by the magnetic field, resulting in the enhancement of the velocity. The impact of porosity on the fluid flow is depicted in Fig. 4c. The escalation in Darcy number (Da) causes an increment in the permeability of the medium which aids the fluid to flow, causing an upsurge in the fluid velocity. Figure 4d compares the present velocity profile with the results of Li et al. [8] under the corresponding limiting conditions. The close agreement between the two profiles validates the accuracy of the present analytical solution.

Figure 5 verifies the same behaviour as observed in Fig. 3a. Figure 6 presents velocity contours for increasing Darcy number and shows the enhancement of velocity due to reduced porous resistance, whereas Fig. 7 presents velocity contours for increasing magnetic parameter and confirms the suppressing effect of the Lorentz force. These contour trends are consistent with the corresponding velocity-profile results in Fig. 4.

6.2. Temperature distribution

Figures 8a and b show the impact of the source parameter (S) and Peclet number (Pe) on the temperature profile, respectively. The rise in temperature with the increase in S is due to the fact that the increment in the source parameter adds more energy to the fluid, inducing an upsurge in the fluid temperature. In microchannel flows, an increase in the Peclet number indicates stronger convective heat transfer relative to conductive heat transfer. As Pe increases, the fluid transports thermal energy more effectively along the flow direction. This causes heat to accumulate within the fluid bulk, raising the overall temperature.

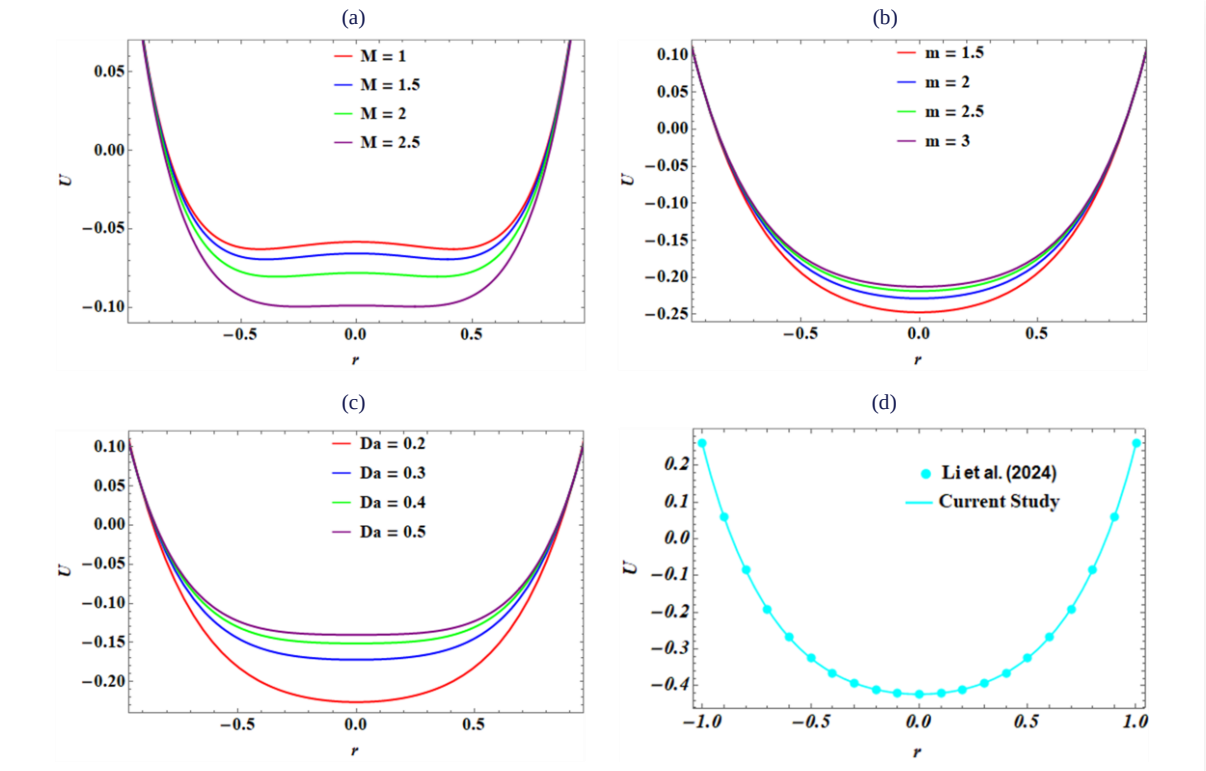


Fig. 4. Velocity profile change with magnetic parameter (a), Hall parameter (b), Darcy number (c), and the comparison with the previous study (d).

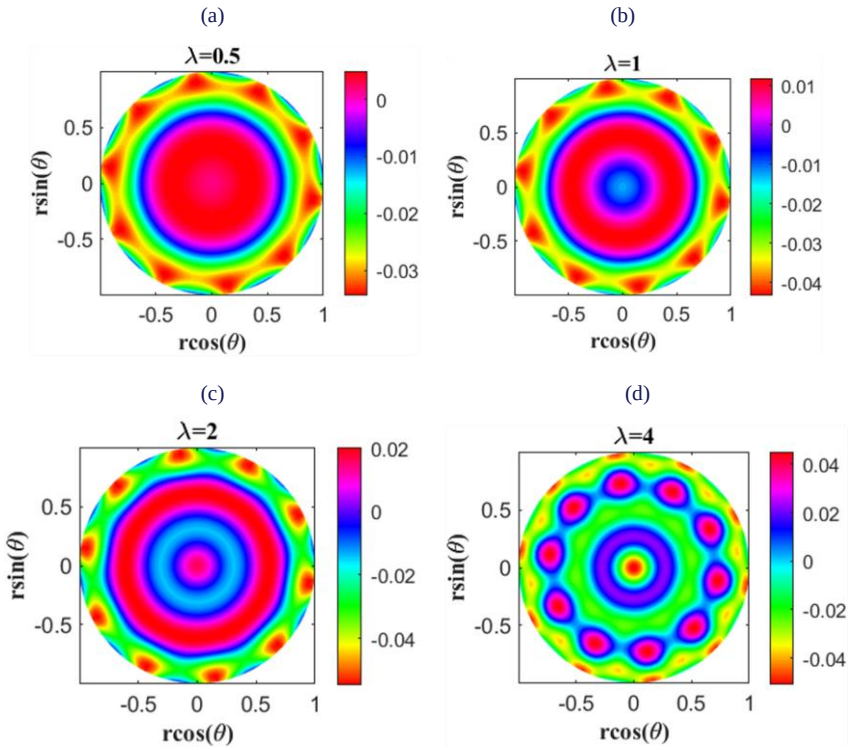


Fig. 5. Velocity contours for various values of relaxation time: (a) λ = 0.5, (b) λ = 1, (c) λ = 2, (d) λ = 4.

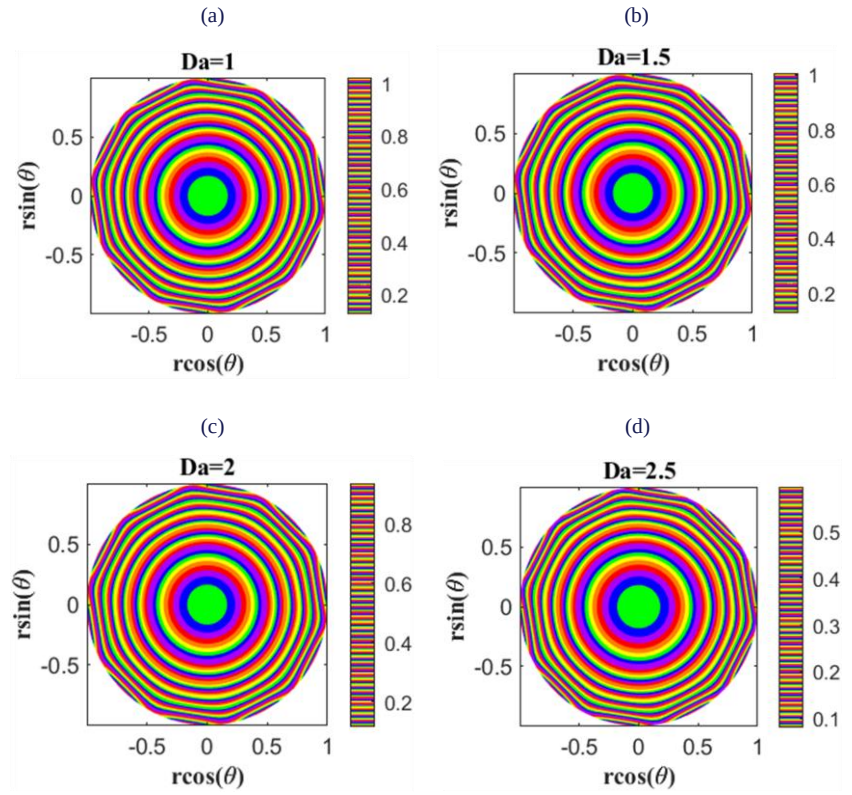


Fig. 6. Velocity contours for various values of Darcy number: (a) Da = 1, (b) Da = 1.5, (c) Da = 2, (d) Da = 2.5.

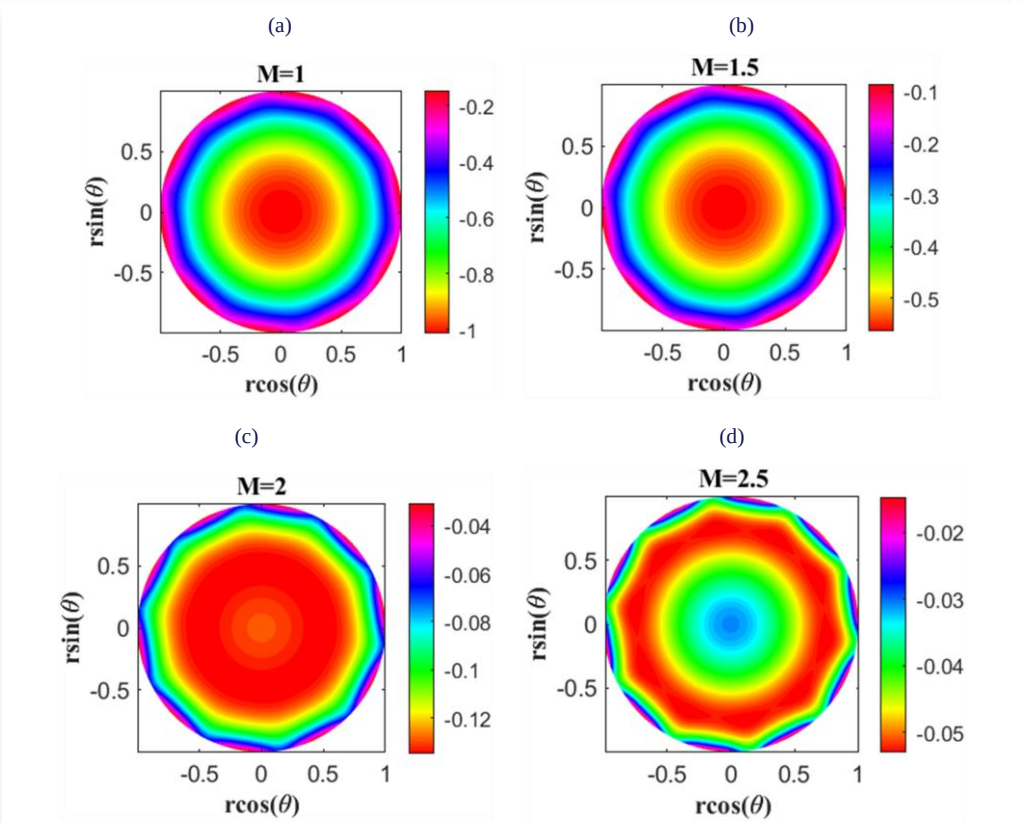


Fig. 7. Velocity contours for various values of magnetic parameter: (a) M = 1, (b) M = 1.5, (c) M = 2, and (d) M = 2.5.

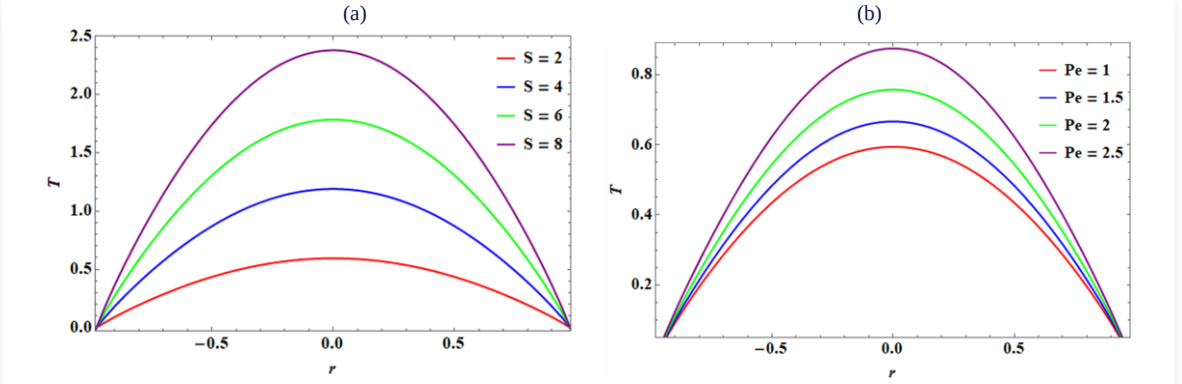


Fig. 8. Temperature profile change with source parameter (a) and Peclet number (b).

Figures 9 and 10 present the temperature contours for the variation in Peclet number and heat source parameter, respectively. It is observed that the temperature rises with the increment in both parameters, verifying the trend shown in Fig. 8. The increase in the source parameter adds significant energy to the fluid, causing an increase in the temperature, whereas the increment with increasing Peclet number shows that the fluid transmits the energy more efficiently.

Table 1 depicts the effect of the relaxation time, Darcy number and Hall parameter on the shear stress of the fluid. It is observed that shear stress rises with an increase in relaxation time, while it declines as the Darcy number and Hall parameter increase. Table 2 is produced to portray the influence of the source parameter and Peclet number on the Nusselt number. It is noted that the Nusselt number upsurges for both parameters, as the increase in the source parameter and Peclet number enhances the heat transfer, causing an increase in the Nusselt number.

7. Conclusions

In this study, the magnetised oscillatory flow of a Maxwell fluid through a porous circular microchannel with a rough wall, considering both no-slip and slip boundary conditions with the Hall effect, is analysed. In addition to examining the influence of slip length, wave number and wall roughness on the velocity and volumetric flow rate, we extended the analysis to include the effects of the magnetic parameter, Hall effect and Darcy number on the velocity profiles, as well as the Peclet number and heat

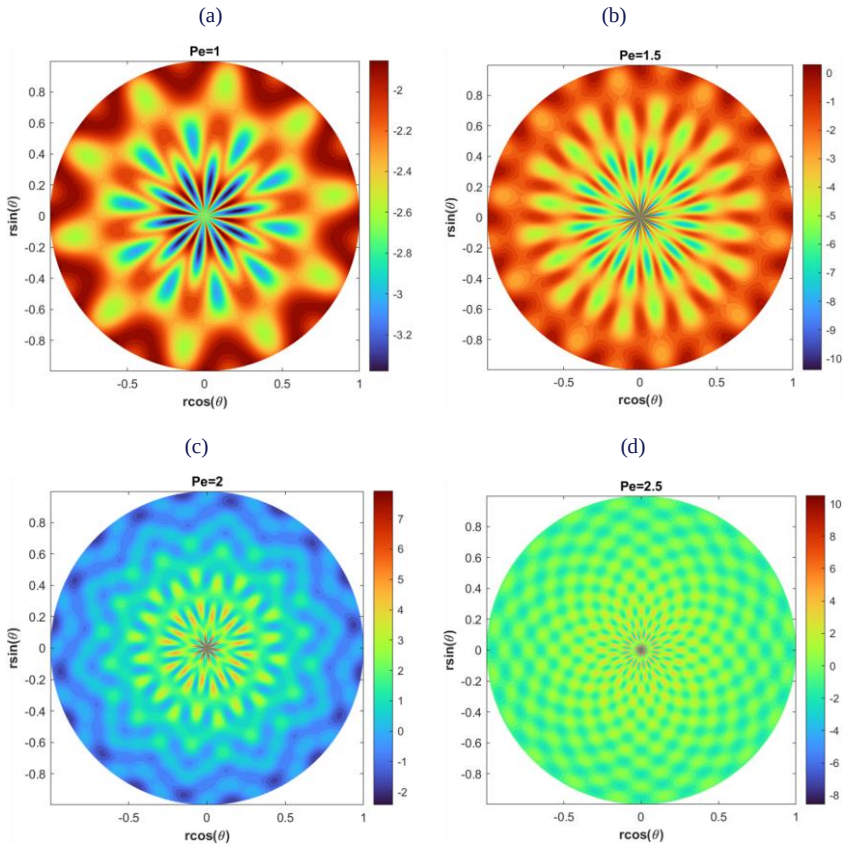


Fig. 9. Temperature contours for various Peclet numbers: (a) Pe = 1, (b) Pe = 1.5, (c) Pe = 2, and (d) Pe = 2.5.

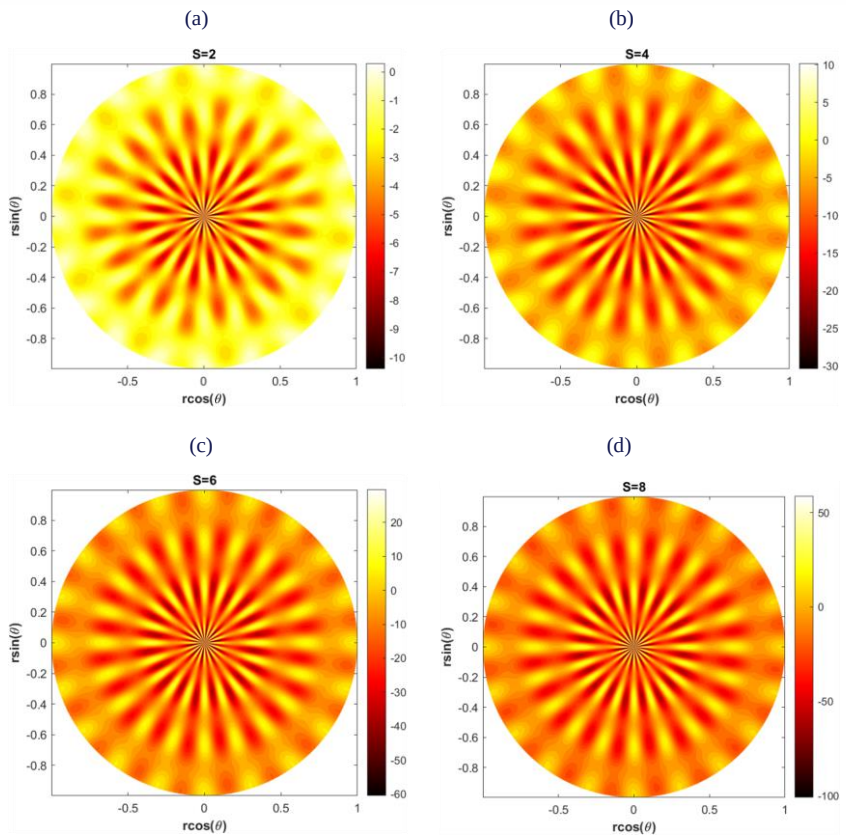


Fig. 10. Temperature contours for various values of heat source/sink parameter:
(a) S = 2, (b) S = 4, (c) S = 6, and (d) S = 8.

Table 1. The impact of relaxation time (λ), Darcy number (Da), and Hall parameter (m) on the shear stress (τ).

Parameters			Shear stress
Relaxation time	Darcy number	Hall parameter	
2	0.2	2.0	1.53776
3	0.2	2.0	1.45982
4	0.2	2.0	1.51182
5	0.2	2.0	1.63513
6	0.2	2.0	1.81535
2	0.2	1.5	1.55540
–	0.3	–	1.49933
–	0.4	–	1.48191
–	0.5	–	1.47420
–	0.6	–	1.47007
2	0.2	1.5	1.55540
–	–	2.0	1.53776
–	–	2.5	1.52867
–	–	3.0	1.52347
–	–	3.5	1.52025

Table 2. The impact of the source parameter (S) and Peclet number (Pe) on the Nusselt number.

Parameters		Nusselt number
Source parameter	Peclet number	
1.0	2.0	0.81177
1.5	–	1.32176
2.0	–	1.76234
2.5	–	2.20293
3.0	–	2.64325
3.5	–	3.0841
2.0	1.0	1.48937
–	1.5	1.61065
–	2.0	1.76234
–	2.5	1.95782
–	3.0	2.21966
–	3.5	2.58916

source/sink parameter on the thermal characteristics of the flow. The following are the key findings.

- Velocity increases with the slip length and wall roughness at a low Reynolds number.
- The magnetic field suppresses velocity due to the Lorentz force, while the Hall effect causes a rise in the fluid velocity.
- A heat source and a higher Peclet number lead to an increase in the temperature profile.
- The Nusselt number increases with an increase in the source parameter and the Peclet number.
- Shear stress increases for Maxwell's fluid parameter while it declines with an increase in porosity and Hall current.

References

[1] Ray, S., Ünsal, B., & Durst, F. (2012). Development length of sinusoidally pulsating laminar pipe flows in moderate and high Reynolds number regimes. *International Journal of Heat and Fluid Flow*, 37, 167–176. doi: 10.1016/j.ijheatfluidflow.2012.06.001

[2] Astakhov, S., Fujiwara, N., Gulay, A., Tsukamoto, N., & Kurths, J. (2013). Hopf bifurcation and multistability in a system of phase oscillators. *Physical Review E – Statistical, Nonlinear and Soft Matter Physics*, 88(3), 032908. doi: 10.1103/PhysRevE.88.032908

[3] Aygun, C., & Aydin, O. (2014). Hydrodynamics of piston-driven laminar pulsating flow: Part 1. Developing flow. *Nuclear Engineering and Design*, 274, 164–171. doi: 10.1016/j.nucengdes.2013.11.022

[4] Aygun, C., & Aydin, O. (2014). Hydrodynamics of piston-driven laminar pulsating flow: Part 2. Fully developed flow. *Nuclear Engineering and Design*, 274, 172–180. doi: 10.1016/j.nucengdes.2014.02.020

[5] Sato, M., Hyodo, H., Biwa, T., & Delage, R. (2020). Synchronization of thermoacoustic quasiperiodic oscillation by periodic external force. *Chaos: An Interdisciplinary Journal of Nonlinear Science*, 30(6), 063109. doi: 10.1063/5.0004381

[6] Aslan, E., Ozsaban, M., Ozcelik, G., & Guven, H.R. (2021). A numerical analysis of convection heat transfer and friction factor for oscillating corrugated channel flows. *Heat Transfer Engineering*, 42(3-4), 181–190. doi: 10.1080/01457632.2019.1699287

[7] Wang, J., Deng, X., Jia, D., Lei, J., & Xie, G. (2023). Numerical investigation on effects of rib shapes on oscillating flow and heat transfer in heat exchanger channels. *Thermal Science and Engineering Progress*, 42, 101919. doi: 10.1016/j.tsep.2023.101919

[8] Li, D., Li, H., Ma, L., & Lan, S. (2024). Oscillating flow of Jeffrey fluid in a rough circular microchannel with slip boundary condition. *Chinese Journal of Physics*, 91, 107–129. doi: 10.1016/j.cjph.2024.07.015

[9] Huang, A., Pande, S.D., Feng, J., & Christov, I.C. (2025). Oscillatory flows in three-dimensional deformable microchannels. *Journal of Fluid Mechanics*, 1022, A38. doi: 10.1017/jfm.2025.10771

[10] Duraziński, T., Nowak, A.I., Ishimoto, J., & Pietrowicz, S. (2025). Oscillatory two-phase flow dynamics in capillary tubes under microgravity conditions: Numerical modeling and qualitative analysis of the flow structures. *International Journal of Multiphase Flow*, 184, 105107. doi: 10.1016/j.ijmultiphaseflow.2024.105107

[11] Yu, B., Deng, X., Lei, J., Jia, D., He, S., & Zhang, Y. (2025). Numerical investigation on effects of oil jet angle on oscillating flow and heat transfer characteristics in a piston's dual-cooling galleries. *Applied Thermal Engineering*, 268, 125960. doi: 10.1016/j.applthermaleng.2025.125960

[12] Manthani, N., Nanavath, V.L., & Vedantam, S. (2025). Effect of superimposing oscillatory flow in a milli-channel with static internals – A numerical study. *The Canadian Journal of Chemical Engineering*, 103(2), 927–940. doi: 10.1002/cjce.25389

[13] Jian, Y.-J., Liu, Q.-S., & Yang, L.-G. (2011). AC electroosmotic flow of generalized Maxwell fluids in a rectangular microchannel. *Journal of Non-Newtonian Fluid Mechanics*, 166(21-22), 11581172 1304–1314. doi: 10.1016/j.jnnfm.2011.08.009

[14] Jian, Y., Su, J., Chang, L., Liu, Q., & He, G. (2014). Transient electroosmotic flow of general Maxwell fluids through a slit microchannel. *Zeitschrift für Angewandte Mathematik und Physik*, 65, 435–447. doi: 10.1007/s00033-013-0341-1

[15] Li, X.-X., Yin, Z., Jian, Y.-J., Chang, L., Su, J., & Liu, Q.-S. (2012). Transient electro-osmotic flow of generalized Maxwell fluids through a microchannel. *Journal of Non-Newtonian Fluid Mechanics*, 187-188, 43–47. doi: 10.1016/j.jnnfm.2012.09.005

[16] Escandón, J., Jiménez, E., Hernández, C., Bautista, O., & Méndez, F. (2015). Transient electroosmotic flow of Maxwell fluids in a slit microchannel with asymmetric zeta potentials. *European Journal of Mechanics – B/Fluids*, 53, 180–189. doi: 10.1016/j.euromechflu.2015.05.001

[17] Escandón, J.P., Torres, D.A., Hernández, C.G., Gómez, J.R., & Vargas, R.O. (2022). Transient analysis of the electro-osmotic flow of multilayer immiscible Maxwell fluids in an annular microchannel. *Colloids and Interfaces*, 6(4), 60. doi: 10.3390/colloids6040060

[18] Shah, N.A., Mahsud, Y., Aziz, M., & Tlili, I. (2020). Analytical solutions for unsteady electrohydrodynamics flows of Maxwell fluids in microchannels with circular cross section. *Physics of Fluids*, 32(1), 013107. doi: 10.1063/1.5128688

[19] Yang, X., Wang, S., Zhao, M., & Xiao, Y. (2021). Electroosmotic flow of Maxwell fluid in a microchannel of isosceles right triangular cross section. *Physics of Fluids*, 33(12), 123113. doi: 10.1063/5.0076425

[20] Feng, C., Si, X., Cao, L., & Zhu, B. (2021). The slip flow of generalized Maxwell fluids with time-distributed characteristics in a rotating microchannel. *Applied Mathematics Letters*, 120, 107260. doi: 10.1016/j.aml.2021.107260

[21] Chang, L., Zhao, G., Buren, M., Sun, Y., & Jian, Y. (2024). Alternating current electroosmotic flow of Maxwell fluid in a parallel plate microchannel with sinusoidal roughness. *Micromachines*, 15(1), 4. doi: 10.3390/mi15010004

[22] Jha, B.K., Malgwi, P.B., & Aina, B. (2018). Hall effects on MHD natural convection flow in a vertical microchannel. *Alexandria Engineering Journal*, 57(2), 983–993. doi: 10.1016/j.aej.2017.01.038.

[23] Jha, B.K., & Aina, B. (2018). Impact of induced magnetic field on magnetohydrodynamic (MHD) natural convection flow in a vertical annular micro-channel in the presence of radial magnetic field. *Propulsion and Power Research*, 7(2), 171–181. doi: 10.1016/j.jppr.2018.04.004

[24] Jha, B.K., & Malgwi, P.B. (2019). Hall current and ion-slip effects on free convection flow in a vertical microchannel with an induced magnetic field. *Heat Transfer – Asian Research*, 48(8), 3812–3830. doi: 10.1002/htj.21569

[25] Jha, B.K., & Malgwi, P.B. (2020). Hall and ion-slip effects on MHD mixed convection flow in a vertical microchannel with asymmetric wall heating. *Engineering Reports*, 2(9), e12241. doi: 10.1002/eng2.12241

[26] Roja, A., & Gireesha, B.J. (2020). Hall effects on MHD couple stress fluid flow through a vertical microchannel subjected to heat generation: A numerical study. *Heat Transfer*, 49(8), 4738–4758. doi: 10.1002/htj.21850

[27] Sadiq Basha, P.M., Veera Krishna, M., & Nagarathna, N. (2020). Hall and ion-slip effects on steady MHD free convective flow through a porous medium in a vertical microchannel. *Heat Transfer*, 49(8), 4264–4280. doi: 10.1002/htj.21826

[28] Kundu, B., & Saha, S. (2022). Review and analysis of electromagnetohydrodynamic flow and heat transport in microchannels. *Energies*, 15(19), 7017. doi: 10.3390/en15197017

[29] Bilal, M., Javid, K., & Ali, N. (2023). Unsteady flow of hybrid fluid via peristaltic pumping in wavy micro-channel under electric and magnetic field effects: An application of Hall device and slip boundary. *Proceedings of the Institution of Mechanical Engineers, Part E: Journal of Process Mechanical Engineering*, 237(6), 2157–2170. doi: 10.1177/09544089231157512

[30] Goyal, K., & Srinivas, S. (2023). Entropy generation analysis for hydromagnetic two-layered pulsatile immiscible flow with Joule heating and first-order chemical reaction. *Case Studies in Thermal Engineering*, 47, 103046. doi: 10.1016/j.csite.2023.103046

[31] Roja, A., Saadeh, R., Kumar, R., Qazza, A., Khan, U., Ishak, A., & Pop, I. (2024). Ramification of Hall effects in a non Newtonian model past an inclined microchannel with slip and convective boundary conditions. *Applied Rheology*, 34(1), 2450046. doi: 10.1515/arh-2024-0010

[32] Padma Devi, M., Srinivas, S., & Vajravelu, K. (2024). Entropy generation in two-immiscible MHD flow of pulsating Casson fluid in a vertical porous space with slip effects. *Journal of Thermal Analysis and Calorimetry*, 149, 7449–7468. doi: 10.1007/s10973-024-13337-8

[33] Bala Anasuya, J., & Srinivas, S. (2024). Heat transfer characteristics of magnetohydrodynamic two-fluid oscillatory flow in an inclined channel with saturated porous medium. *Proceedings of the Institution of Mechanical Engineers, Part E: Journal of Process Mechanical Engineering*, 238(1), 427–440. doi: 10.1177/09544089221146364

[34] Anasuya, J.B., Srinivas, S., & Merugu, V. (2025). Interaction of pulsatile and peristaltic flow of a particle-fluid suspension with thermal effects. *International Communications in Heat and Mass Transfer*, 163, 108728. doi: 10.1016/j.icheatmasstransfer.2025.108728